JBC RESEARCH ARTICLE

DNA polymerase η promotes nonhomologous end joining upon etoposide exposure dependent on the scaffolding protein Kap1

Received for publication, September 17, 2021, and in revised form, March 16, 2022 Published, Papers in Press, March 23, 2022,
https://doi.org/10.1016/j.jbc.2022.101861

Xiaolu Ma[1,2], Chen Wang[3], Bo Zhou[4], Zina Cheng[1], Zhiyong Mao[3], Tie-Shan Tang[2,5,6,*], and Caixia Guo[4,*]

From the [1]College of Biomedical Engineering, Taiyuan University of Technology, Taiyuan, China; [2]State Key Laboratory of Membrane Biology, Institute of Zoology, University of Chinese Academy of Sciences, Chinese Academy of Sciences, Beijing, China; [3]Clinical and Translational Research Center of Shanghai First Maternity & Infant Hospital, Shanghai Key Laboratory of Signaling and Disease Research, School of Life Sciences and Technology, Tongji University, Shanghai, China; [4]CAS Key Laboratory of Genomics and Precision Medicine, Beijing Institute of Genomics, University of Chinese Academy of Sciences, Chinese Academy of Sciences/China National Center for Bioinformation, Beijing, China; [5]Institute for Stem Cell and Regeneration, Chinese Academy of Sciences, Beijing, China; 6Beijing Institute for Stem Cell and Regenerative Medicine, Beijing, China

Edited by Patrick Sung

DNA polymerase eta (Pol η) is a eukaryotic member of the Y-family of DNA polymerase involved in translesion DNA synthesis and genome mutagenesis. Recently, several translesion DNA synthesis polymerases have been found to function in repair of DNA double-strand breaks (DSBs). However, the role of Pol η in promoting DSB repair remains to be well defined. Here, we demonstrated that Pol η could be targeted to etoposide (ETO)-induced DSBs and that depletion of Pol η in cells causes increased sensitivity to ETO. Intriguingly, depletion of Pol η also led to a nonhomologous end joining repair defect in a catalytic activity–independent manner. We further identified the scaffold protein Kap1 as a novel interacting partner of Pol η, the depletion of which resulted in impaired formation of Pol η and Rad18 foci after ETO treatment. Additionally, overexpression of Kap1 failed to restore Pol η focus formation in Rad18-deficient cells after ETO treatment. Interestingly, we also found that Kap1 bound to Rad18 in a Pol η-dependent manner, and moreover, depletion of Kap1 led to a significant reduction in Rad18–Pol η association, indicating that Kap1 forms a ternary complex with Rad18 and Pol η to stabilize Rad18–Pol η association. Our findings demonstrate that Kap1 could regulate the role of Pol η in ETO-induced DSB repair *via* facilitating Rad18 recruitment and stabilizing Rad18–Pol η association.

DNA polymerase eta (Pol η) is a well-known member of Y-family DNA polymerases that are involved in translesion DNA synthesis (TLS) to maintain genome integrity. Specifically, Pol η accumulates at stalled replication forks and proceed accurately with cyclobutane pyrimidine dimers generated by ultraviolet (UV) radiation. Pol η can also efficiently replicate across cisplatin GpG adducts, which is closely related to cisplatin resistance of tumor cells (1–4). Inherited truncating mutations in Pol η are primarily associated with photosensitivity and skin cancer (5, 6). Compelling evidence reveals that DNA damage–induced Pol η focus formation during TLS is stringently regulated by protein post-translational modification and protein–protein interaction, especially its binding to the mono-ubiquitinated proliferating cell nuclear antigen (PCNA) (mUb-PCNA) that is catalyzed by ubiquitin E3 ligase Rad18 (7, 8). Beyond its canonical role in TLS, Pol η has been reported to participate in DNA synthesis in several situations such as replication of common fragile sites, nucleotide excision repair, and re-replication (9–11). Particularly, Pol η has been implicated to function in homologous recombination (HR), a high-fidelity repair pathway mainly occurring in the S and G2 phases of the cell cycle for DNA double-strand breaks (DSBs) that are the most toxic type of DNA lesions, based on both biochemical analyses and genetic studies performed in chicken DT40 cells (12, 13). However, it remains a mystery as for the role of Pol η in DSB repair.

Acute DSB formation is the central mechanism of radiotherapy and chemotherapeutic agents for many cancer treatments. Etoposide (ETO), a type II topoisomerase (Top2) inhibitor, is a broad-spectrum anticancer drug and a potent inducer of DSBs by interfering with the normal enzymatic cleavage and religation reaction with Top2 covalently bound to the 5′ end of the DNA (14, 15). In addition to HR, nonhomologous end joining (NHEJ), another major DSB repair pathway, also plays an important role upon ETO exposure (16, 17). Actually, NHEJ, which is active throughout the cell cycle, is more preferentially employed in mammalian cells to quickly repair DSBs in the genome (18). In NHEJ pathway, DSBs are first recognized by the Ku70–Ku80 heterodimer followed by recruiting other NHEJ proteins such as DNA-dependent protein kinase catalytic subunit (DNA-PKcs), DNA polymerase μ, and X-ray repair cross-complementing protein 4 to promote the joining of DSB ends (19). Emerging data show the importance of Pol η in influencing the therapeutic outcome and chemoresistance of platinum-based anticancer drugs

* For correspondence: Tie-Shan Tang, tangtsh@ioz.ac.cn; Caixia Guo, guocx@big.ac.cn.

(20–22). It is still obscure whether Pol η participates in ETO-induced damage repair and affects its killing effect.

In the current study, we found that Pol η could accumulate at both laser- and ETO-induced DSB sites and promote NHEJ repair. Depletion of Pol η delayed DSB repair process and sensitized cells to ETO treatment. Through mass spectrometry (MS), we identified Krüppel-associated box–associated protein 1 (Kap1) to be a new partner of Pol η. Knockdown of Kap1 reduced Pol η accumulation at DSBs induced by ETO, which could be rescued by ectopically expressed Kap1. However, Kap1 supplementing failed to rescue ETO-induced Pol η accumulation in Rad18-knockout (KO) cells. Interestingly, we found that Kap1 is required for optimal Rad18 accumulation at ETO-induced damage sites, whose deficiency led to a significant reduction in Rad18 focus formation. Moreover, Kap1 also associates with Rad18 in a Pol η–dependent fashion. And the association between Pol η and Rad18 was enhanced by ETO treatment, while dramatically decreased upon Kap1 depletion, indicating that Kap1 binds to Rad18 and Pol η, forming a ternary complex to stabilize Rad18–Pol η association. Notably, the stimulatory role of Kap1 in Rad18–Pol η association is independent of Rad18 phosphorylation on S409/S434 sites. Collectively, we revealed a novel role of Pol η in ETO-induced DSB repair, which is regulated by Kap1 in a Rad18-dependent manner.

Results

Pol η accumulates at DSB sites and promotes ETO-induced DSB repair

Given that Pol η not only accumulates at DNA lesions upon UV or cisplatin exposure but also extends D-loop *in vitro* (13), we hypothesized that Pol η might also be recruited to DSBs *in vivo*. We first expressed GFP-fused Pol η into U2OS cells and treated the cells with laser microirradiation to examine the accumulation of Pol η to laser-induced damage sites. As expected, a rapid accumulation of Pol η at laser tracks marked by 53BP1 (p53-binding protein 1) or γH2AX, two representative biomarkers of DSBs, was found (Fig. S1*A*). Considering that Ataxia telangiectasia mutated (ATM) kinase is a vital and early transducer of DSB signals, we then treated cells with ATM inhibitor Ku55933 prior to microirradiation and found that ATM inhibition resulted in an obvious decrease of Pol η recruitment (Fig. S1*B*), suggesting that Pol η accumulates at laser-induced damage sites partially depending on ATM. Given that ETO is commonly used to cure cancer by inducing DSBs *in vivo*, we wonder whether Pol η could localize to ETO-induced DSB sites in cells and further affect the efficacy of ETO treatment. To investigate the role of Pol η upon ETO treatment, we transfected GFP-Pol η into U2OS cells and detected its focus formation after ETO exposure. An obvious assembly of GFP-Pol η was found after ETO treatment (Fig. 1, *A* and *B*), suggesting that Pol η might participate in ETO-induced damage repair. 53BP1 focus formation is an early event in the cellular response to DSBs, whose disappearance can reflect DSB repair progression. To understand the functional importance of Pol η in repairing ETO-induced DSBs, we investigated the time course of 53BP1 focus dispersion in Pol η–proficient (MRC5) and Pol η–deficient (XPV) cells post ETO treatment. The percentages of cells with 53BP1 foci were similar between MRC5 and XPV cells immediately after ETO treatment (55% and 54.9%, respectively). However, compared to MRC5 cells, XPV cells displayed a much slower rate in 53BP1 focus dispersion after ETO treatment (Fig. S1*C*), with the proportions of 53BP1 foci–positive cells in XPV being significantly higher than those in MRC5 cells (43.3% *versus* 30.5% at 2 h, 37.1% *versus* 20.7% at 10 h, and 22.8% *versus* 5.1% at 30 h). To exclude the possibility that the delayed 53BP1 focus dispersion in XPV cells was caused by nonisogenic effect, we repeated the experiment in MRC5 cells with Pol η–stable knockdown. Consistently, depletion of Pol η also caused a significant delay in removal of 53BP1 foci, resulting in a higher proportion of 53BP1 foci–positive cells and a higher 53BP1 foci number per cell after ETO treatment (Fig. 1, *C–E*). These data indicate that Pol η deficiency impairs ETO-induced DSB repair. We then examined the dynamics of Rad51 focus formation and dispersion in XPV cells to assess its HR activity after ETO treatment. Supporting the role of Pol η in a late step in HR, we observed a significantly higher extent of Rad51 foci at 10 h and 30 h post ETO in XPV cells than that in MRC5 cells (Fig. S1*D*). Interestingly, no significant difference in Rad51 focus formation between MRC5 and XPV cells could be detected at 0 h and 2 h post ETO (Fig. S1*D*).

Pol η deficiency causes impaired NHEJ efficiency and increased sensitivity to ETO

To determine whether NHEJ pathway also contributes to the DSB repair defect caused by Pol η deficiency, we treated shPol η-MRC5 cells with ETO and costained 53BP1 with S/G2 cell cycle marker cyclin A. As is shown in Figure 1*F*, although there were scanty 53BP1 foci existing in cyclin A–positive cells, most unrepaired DSBs persisted in cyclin A–negative cells, supporting that Pol η knockdown resulted in a DSB repair defect in G1, when NHEJ but not HR is operative. We next examined whether Pol η affects NHEJ repair through an integrated DR-GFP reporter system established in HeLa cells (23) (Fig. S2*A*). We observed a significant increase in GFP signal when Flag-Pol η was overexpressed compared to Flag-vector (Fig. S2*B*). Consistently, knockdown of Pol η resulted in an obvious reduction in NHEJ efficiency (Fig. S2*C*), which could be restored when Pol η knockdown cells were complemented with Flag-Pol η (Fig. 2*A*). These data support that Pol η could accumulate at ETO-induced damage sites to facilitate NEHJ repair. To further test whether the DNA polymerase activity of Pol η is required for its role in NHEJ, we generated a catalytically inactive Pol η mutant (D13A/E22A/D115A/E116A, Pol η-CI) (24). We found that, similar to Pol η wildtype (Pol η-WT), Pol η-CI still accumulated at ETO-induced DSB sites (Fig. 2*B*), and overexpression of Pol η-CI could cause a comparable increase in NHEJ efficiency as Pol η-WT (Fig. 2*C*). Thus, the role of Pol η in promoting ETO-induced NHEJ repair can be independent of its catalytic activity.

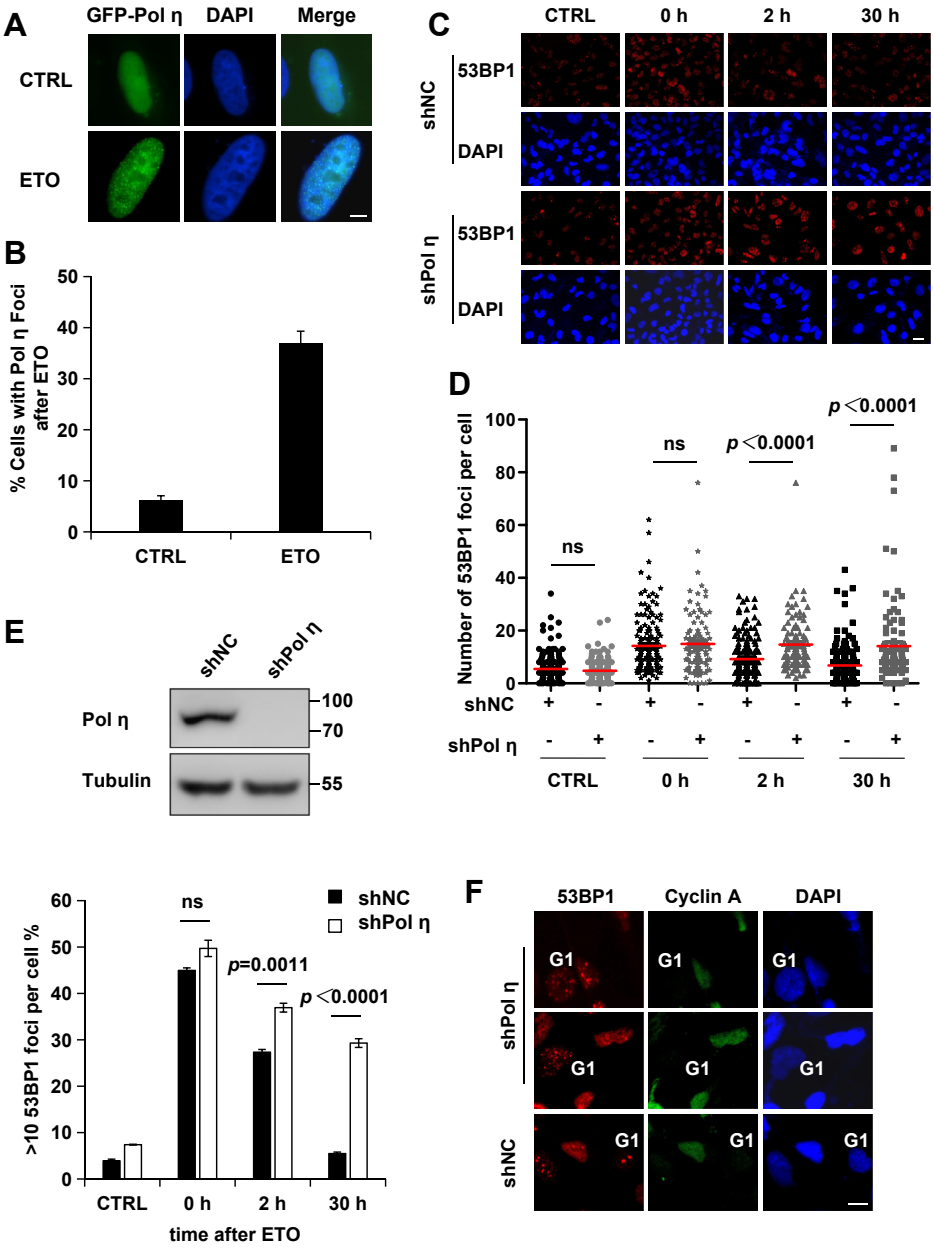

Figure 1. Pol η accumulates at ETO-induced damage sites and promotes NHEJ repair. *A*, localization of GFP-Pol η after ETO treatment. GFP-Pol η–transfected U2OS cells were treated with ETO (2.5 μM) and further incubated for 24 h. The cells were then fixed and DAPI-stained. Scale bars: 3 μm. *B*, the proportions of GFP-Pol η–expressing cells with more than 30 foci were determined. Data represent means ± SEM from three independent experiments. *C*, representative images of cells stained with DAPI and 53BP1 after ETO treatment. ShNC-treated and shPol η–treated MRC5 cells were treated with 50 μM ETO for 30 min and further cultured. At the indicated time points, cells were treated with 0.5% Triton-X100 for 10 min followed by immunofluorescence. Scale bars: 10 μm. *D*, quantification of the number of 53BP1 foci in (*C*). For each cell line at each time point, at least 100 cells were measured. *E*, quantification of the percentage of cells with more than 10 53BP1 foci. The upper panels show immunoblots indicating the Pol η levels. Tubulin: loading control. For each cell line at each time point, at least 200 cells were counted. Data represent means ± SEM from three independent experiments. *F*, representative images of cells costained with 53BP1 and cyclin A after ETO treatment. ShNC- and shPol η-MRC5 cells were treated with 50 μM ETO for 30 min and further cultured for 30 h, followed by immunofluorescence. G1 represents cyclin A–negative cells. Scale bars: 5 μm. DAPI, 4, 6-diamidino-2-phenylindole; ETO, etoposide; NHEJ, nonhomologous end joining.

To address the functional significance of Pol η recruitment to ETO-induced DSBs, we next tested the effect of Pol η deficiency on cellular survival after ETO treatment. We found that Pol η–depleted U2OS or MRC5 cells displayed an increased sensitivity to ETO treatment (Figs. S2*D* and 2, *D* and *E*). Consistently, compared to MRC5, XPV (Pol η–deficient) cells exhibited an increased sensitivity to ETO, which could be rescued by complementary GFP-Pol η (Fig. 2, *D* and *E*). These data suggest that Pol η plays an essential role in promoting cell survival after ETO. It is known that DNA damage caused by ICRF-193 (another Top2 inhibitor) is predominantly repaired by the NHEJ pathway (25). To further support the role of Pol η in NHEJ, we examined the viability of XPV cells to ICRF-193. Indeed, XPV cells displayed a significant decrease in viability following exposure to ICRF-193 compared to MRC5 and

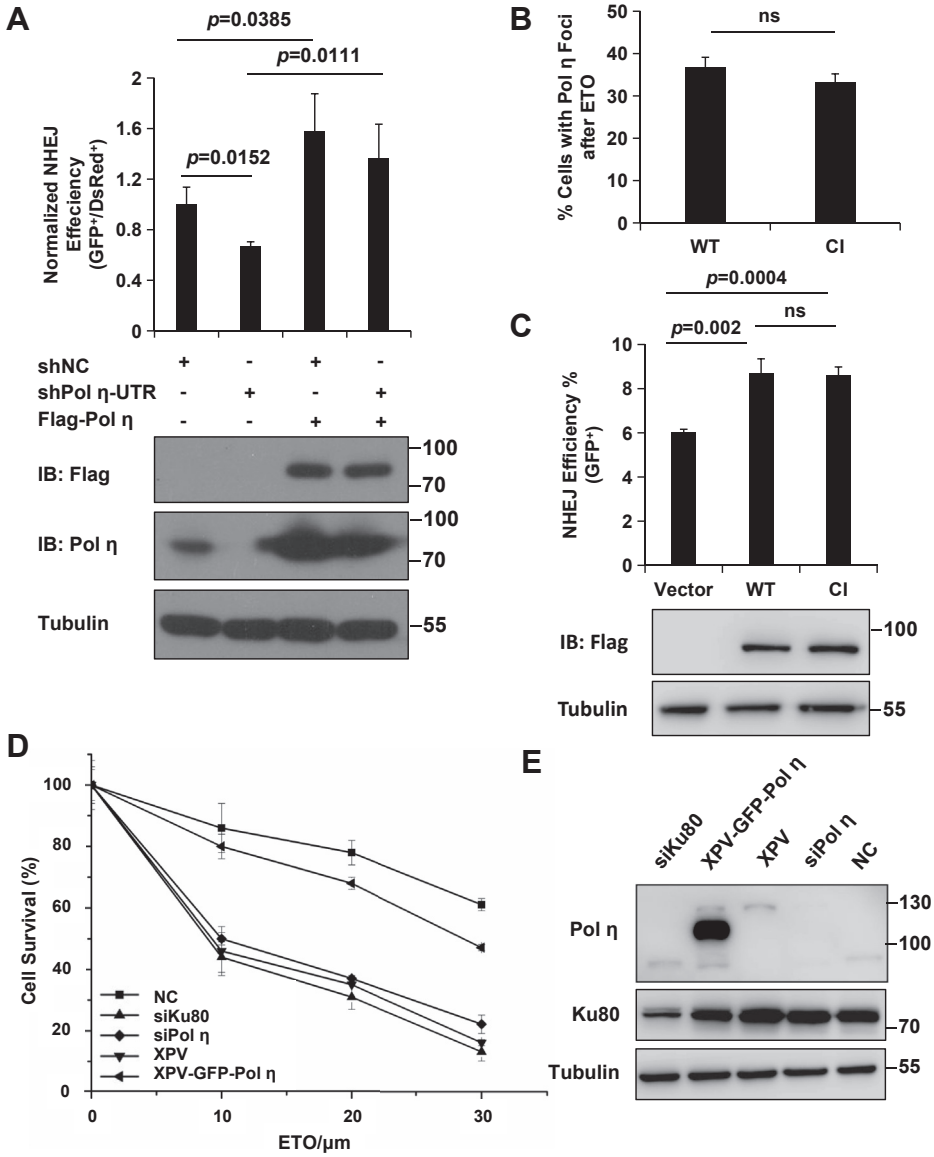

Figure 2. Pol η deficiency leads to NHEJ repair defect and cellular hypersensitivity to ETO. *A*, Pol η shRNA–treated cells complemented with Flag-Pol η or not were transfected with NHEJ reporter (I-SceI endonuclease encoding plasmid and pDsRed2-N1). NHEJ repair efficiency ($GFP^+/DsRed^+$) were analyzed by FACS after 96 h. The lower panels show the Pol η levels through immunoblotting. Tubulin: loading control. *B*, the recruitment of Pol η to ETO-induced DSBs is independent of its catalytic activity. The proportions of GFP-Pol η WT- or CI (catalytic inactive) mutant-expressing cells with more than 30 foci were determined. Data represent means ± SEM from three independent experiments. *C*, the role of Pol η in NHEJ is independent of its catalytic activity. EJ5 cells overexpressing Flag-vector, or Flag-Pol η WT, or CI were transfected with I-SceI endonuclease. NHEJ repair efficiency (GFP^+) was analyzed by FACS after 48 h. The lower panels show immunoblots indicating the Pol η levels in different conditions. *D*, MRC5 (NC, siPol η, and siKu80), XPV, and GFP-Pol η–complemented XPV (XPV-GFP-Pol η) cells were treated with indicated ETO and further incubated for 7 to 10 days. The number of clones was determined. Surviving fraction was expressed as a percentage of mock-treated cells. Experiment was repeated three times, giving similar results. The representative curve is shown. Error bar: s.d., n = 3. *E*, immunoblots indicating the Pol η and Ku80 levels in (*D*). Tubulin: loading control. DSB, double-strand break; ETO, etoposide; FACS, fluorescence activated cell sorting; NHEJ, nonhomologous end joining.

GFP-Pol η–complemented XPV (XPV-GFP-Pol η) cells (Fig. S2*E*). As Pol η functions in the TLS pathway, we wonder whether the role of Pol η in DSB repair is related to its classical TLS bypass activity. Given that mUb-PCNA catalyzed by the principal E3 ubiquitin ligase Rad18 on lysine 164 (K164) provides a landing platform for the recruitment of TLS polymerases to DNA lesions allowing bypass of replication-blocking lesions (26, 27), we treated cells with UV irradiation and several DSB-inducing agents including ETO, ICRF-193, and bleomycin to examine cellular mUb-PCNA levels. As is shown, although UV irradiation induced a significant increase of mUb-PCNA in Rad18 WT but not KO cells, no obvious mUb-PCNA could be detected after ETO, ICRF-193, and bleomycin treatments (Fig. S2*F*). Collectively, these results suggest that Pol η plays a distinct role in promoting NHEJ, which could be dissociable from its TLS function.

Kap1 is a novel Pol η–interacting protein

To explore the potential proteins that engage Pol η to ETO-induced damage sites, we overexpressed Flag-Pol η in HEK293T cells and performed chromatin immunoprecipitation

experiments followed by MS. We identified a subset of Pol η–associating proteins that are involved in DNA damage repair in the immunoprecipitates (Table S1). Besides the well-known Pol η partners, such as Rad18 and PCNA, several other proteins involved in DSB repair including DNA-dependent protein kinase catalytic subunit (DNA-PKcs), Ku autoantigen, 70 kDa (Ku70), Kap1, and poly(ADP-ribose) polymerase 1 (PARP1) were identified (Fig. 3*A*). We then performed coimmunoprecipitation (Co-IP) assay to validate the associations between Pol η and DNA-PKcs, Ku70, Kap1, or PARP1. Endogenous DNA-PKcs and Kap1 were found to bind to Flag-Pol η specifically, whereas Ku70 and PARP1 failed to be immunoprecipitated efficiently by Flag-Pol η (Fig. 3*B*). In turn, Flag-Pol η could also be immunoprecipitated by endogenous Kap1 (Fig. S3*A*). Considering that DNA-PKcs forms the active DNA-PK holoenzyme with Ku70–Ku80 heterodimer to play crucial roles in NHEJ repair, we then checked whether the DNA-PKcs kinase activity is required for Pol η accumulation at DSB sites. As is shown in Fig. S3*B*, treatment with DNA-PKcs kinase inhibitor NU7026 did not cause an obvious reduction in Pol η focus formation upon ETO exposure, suggesting that DNA-PKcs kinase activity is not required for Pol η recruitment at ETO-induced DSBs.

It is known that ATM-induced Kap1 phosphorylation at Ser824 (S824p) in response to DNA damage facilitates local chromatin relaxation (28). Given that the recruitment of Pol η to laser-induced damage sites is partially impaired by ATM inhibitor, we assume that Kap1 might regulate the role of Pol η in NHEJ repair. To prove this, we first determined whether the Kap1–Pol η interaction is direct by checking the binding between purified glutathione S-transferase (GST)–tagged Kap1 and His-tagged Pol η *in vitro*. Indeed, His-Pol η was pulled down by GST-Kap1 (Fig. 3*C*), confirming that Pol η directly binds to Kap1. Then, we mapped the regions within Pol η responsible for its interaction with Kap1 by using Flag-Pol η and a series of Pol η truncated mutants (1–495, 350–590, and 594–713). As is shown, Pol η-1-495 and Pol η-350–590 mutants displayed relatively strong and weak binding to Kap1, respectively, whereas the association between Kap1 and Pol η-594–713 mutant was absent (Fig. S3*C*), suggesting that the Kap1-binding region of Pol η does not reside within its C-terminal. Furthermore, we constructed a series of Flag-Pol η deletion mutants (K1 (△1–100), K2 (△101–200), K3 (△201–300), K4 (△301–400), K5 (△401–500), K6 (△501–600), and K7 (△601–713) (Fig. S3*D*). Co-IP experiments revealed that the N-terminal 1 to 100 amino acids of Pol η is required for its binding to Kap1 (Fig. 3*D*). As Kap1 can function as an E3 sumo ligase (through PHD domain) and sumoylation of Pol η was reported to regulate its role in response to DNA damage (29, 30), we wondered whether Kap1 sumoylates Pol η *in vivo*. Exogenously expressed Flag-Pol η in Kap1-depleted HEK293T cells was immunoprecipitated to assess its sumoylation through immunoblotting using anti-Sumo antibody. No significant difference in the level of Pol η sumoylation could be detected between siNC- and siKap1-treated cells (Fig. S3*E*). Taken together, these data indicate that Kap1 binds to the N-terminus of Pol η but does not regulate its sumoylation.

Kap1 is required for the recruitment of Pol η to ETO-induced DSB sites

Interestingly, we found that Pol η could colocalize with Kap1 S824p, an early event in DSB repair catalyzed by ATM kinase, at laser-induced tracks (Fig. S4*A*). To examined whether Kap1 regulates Pol η assembly at DSB sites, we transfected siKap1-treated U2OS cells with GFP-Pol η and analyzed its accumulation at laser-induced tracks. As is shown, knockdown of Kap1 led to an obvious reduction of Pol η accumulation at laser-damaged sites compared to negative control (siNC) cells (Fig. 4, *A* and *B*), suggesting that Kap1 regulates the recruitment of Pol η to laser-induced damage sites. In support of it, Kap1 knockdown also resulted in a significant reduction in Pol η focus formation (9.87%) upon ETO treatment, which could be rescued by complementing Myc-Kap1 (36.39%) (Fig. 4, *C* and *D*).

Although the Kap1–Pol η association remains unchanged after ETO exposure (Fig. S4*B*), the proportion of Pol η foci–positive cells post ETO treatment was decreased (41.35% for GFP-Pol η-1-713, 29.80% for GFP-Pol η-301–713, 9.01% for GFP-Pol η-556–713) when its N-terminal domain which is important for Kap1–Pol η association was deleted (Fig. 4, *E* and *F*), suggesting that Kap1–Pol η interaction plays an important role in mediating the recruitment of Pol η to ETO-induced DSB sites. Notably, we also found that the Pol η mutant lacking the C-terminal (GFP-Pol η-1-512), which still interacted with Kap1, failed to be recruited to ETO-induced damage sites (Fig. 4, *E* and *F*), hinting that, besides the Kap1–Pol η association, there exists other mechanism(s) regulating ETO-induced Pol η focus formation. Taken together, these data indicate that Kap1 functions upstream of Pol η to modulate its recruitment to ETO-induced DSB sites.

Kap1 drives Rad18-dependent Pol η focus formation by regulating Rad18 accumulation and enhancing Rad18–Pol η association

Rad18 is known to directly associate with the C-terminal of Pol η and promote UV-induced Pol η focus formation (7). Interestingly, we found that ETO-induced Rad18 foci colocalized with GFP-Pol η at different repair times (2 h and 8 h) (Fig. S5*A*) and Rad18–Pol η association was getting enhanced with increased concentration of ETO exposure (Fig. 5*A*), hinting the role of Pol η in ETO-induced NHEJ repair might also be regulated by Rad18. Such is the case, compared to WT U2OS cells (34.07%) that had a relative higher percentage of Pol η foci–positive cells post ETO treatment, Rad18 KO U2OS cells manifested poor Pol η focus formation (1.25%), which could be largely rescued by complementing with Myc-Rad18 (22.70%) but not Myc-Kap1 (0.63%) (Fig. 5, *B* and *C*). These data hint that Kap1 might modulate Pol η accumulation at DSBs in a Rad18-dependent fashion. In support, we found that Kap1 knockdown caused a dramatic decrease in the

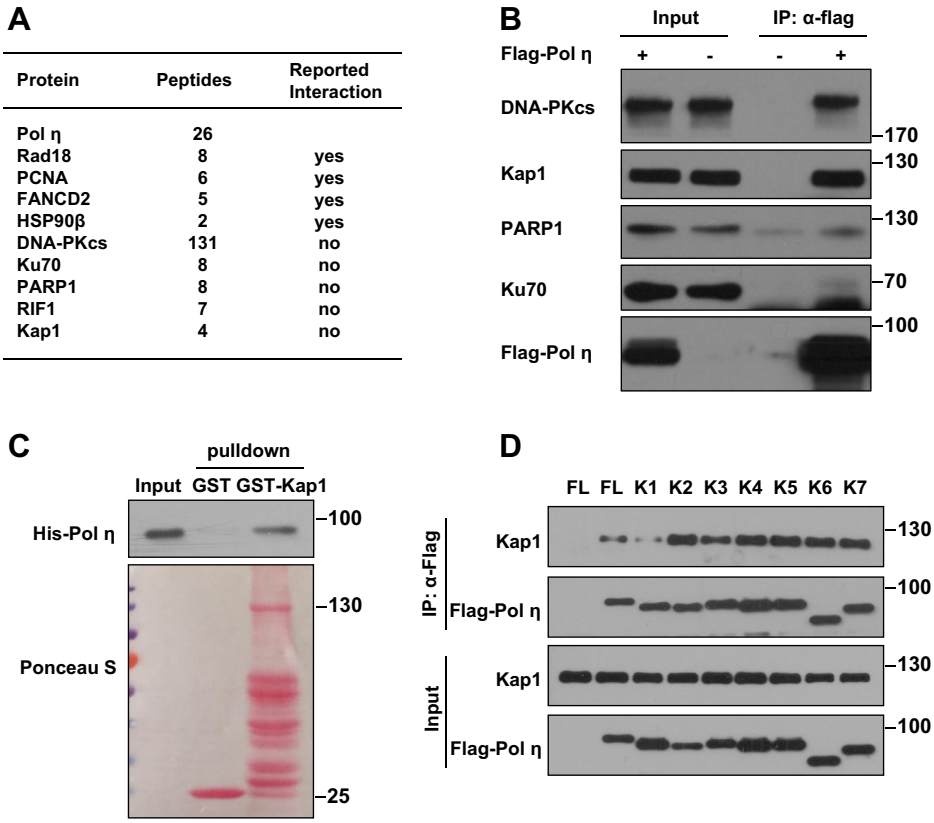

Figure 3. Kap1 is a novel Pol η-interacting protein. *A*, list of proteins identified by mass spectrometry analysis. Triton-insoluble fractions of HEK293T cells expressing Flag-Pol η were lysed and subjected to tandem-affinity purification. Flag-Pol η immunoprecipitated proteins were resolved by SDS-PAGE followed by mass spectrometry analysis. *B*, Kap1 and DNA-PKcs associate with Pol η. HEK293T cells transfected with Flag-Pol η were lysed and immunoprecipitated with anti-Flag M2 beads, followed by immunoblotting with anti-DNA-PKcs, anti-Kap1, anti-PARP1, anti-Ku70, and anti-Flag antibodies. *C*, purified GST or GST-Kap1 proteins were incubated with His-Pol η protein. The bound proteins were resolved by SDS-PAGE and analyzed by immunoblotting with anti-His antibody and staining with Ponceau S. *D*, HEK293T cells expressing full-length (FL) or deletion mutants of Flag-Pol η (K1-K7) were lysed and immunoprecipitated with Flag M2 agarose beads followed by immunoblotting with anti-Kap1 and anti-Flag antibodies.

recruitment of Rad18 post ETO treatment (Fig. 5*D*), indicating that Kap1 modulates Pol η recruitment by facilitating Rad18 focus formation after ETO exposure.

As ETO-induced focus formation of Pol η mutants (GFP-Pol η-301–713 and GFP-Pol η-556–713), which contains Rad18-binding domain but failed to bind Kap1, were decreased compared to that of Pol η full length (GFP-Pol η-1-713) (Fig. 4, *E* and *F*), it is likely that Kap1 can drive Pol η focus formation by regulating Rad18 accumulation and enhancing Rad18–Pol η association after ETO treatment. We then determined the interplay between Kap1–Pol η and Rad18–Pol η associations. Surprisingly, we also detected a clear association between Myc-Rad18 and endogenous Kap1 in HEK293T cells (Fig. 5*E*). To examine whether the Kap1–Rad18 association is Pol η–dependent, we transfected Myc-Kap1 with GFP-Rad18 WT or the mutant (GFP-Rad18-△PID) lacking Pol η–binding domain into HEK293T cells followed by the Co-IP assay. We found that the Kap1-binding capability of GFP-Rad18-△PID was significantly reduced compared to that of GFP-Rad18 WT (Fig. 5*F*), suggesting that Pol η might form a complex with Kap1 and Rad18, to promote the binding of Kap1 and Rad18. To further confirm that, we transfected GFP-Rad18 and Myc-Kap1 into XPV cells (Pol η-deficient) and found that Myc-Kap1 failed to be immunoprecipitated by GFP-Rad18 (Fig. S5*B*). Moreover, we examined the association between Myc-Rad18 and GFP-Pol η full-length or mutant lacking the binding domain for Kap1 (301–713). We found that the association between Myc-Rad18 and GFP-Pol η-301–713 was significantly impaired in comparison to GFP-Pol η full length (1–713) (Fig. 6*A*), indicating that Kap1–Pol η binding promotes Rad18–Pol η association. Similarly, knockdown of Kap1 also reduced the association between Rad18 and Pol η (Fig. S5, *C* and *D*), which could be restored by supplementing with Kap1 (Fig. 6, *B* and *C*). Meanwhile, Pol η still associated with endogenous Kap1 in Rad18 KO cells, accompanied by a slight decrease compared to that in Rad18 WT cells (Fig. 6, *D* and *E*), suggesting that Rad18 is also required for optimal Kap1–Pol η interaction *in vivo*. Taken together, these results reveal that Kap1 forms a ternary complex with Pol η and Rad18, which promotes Rad18-directed Pol η recruitment at ETO-induced DSBs.

Rad18 promotes ETO-induced DSB repair independent of its phosphorylation on S409/S434

We further determined the role of Rad18 and Kap1 in ETO-induced DSB repair. Analogous to Pol η–deficient cells, Rad18 KO cells also displayed a much slower rate in 53BP1 focus

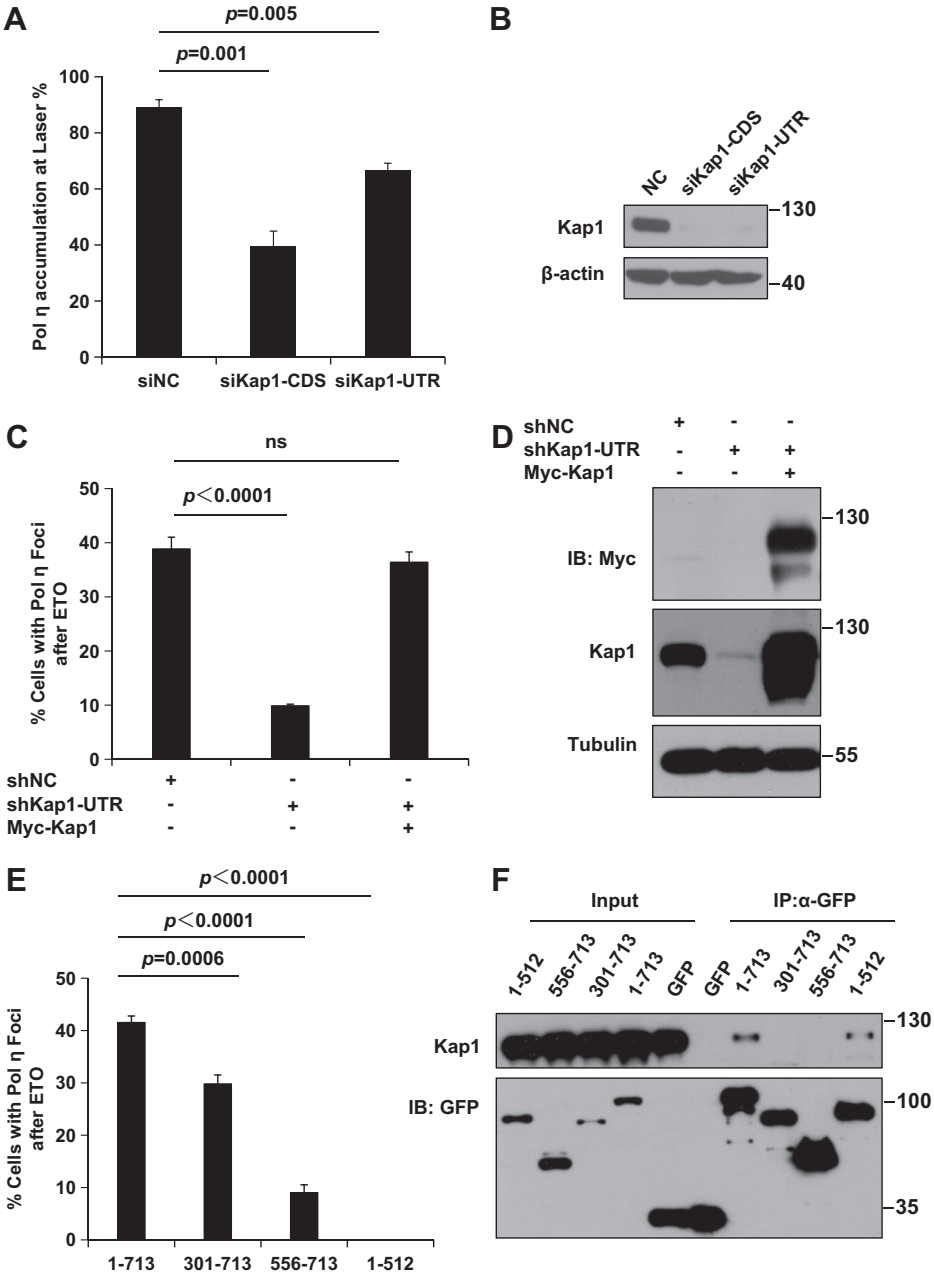

Figure 4. Kap1 depletion impairs the recruitment of Pol η to laser- and ETO-induced damage sites. *A*, U2OS cells were transfected with siKap1 or siNC oligos. Forty-eight hours later, the cells were transfected with GFP-Pol η followed by microirradiation. The proportion of cells with Pol η accumulation was quantified. Data represent means ± SEM from three independent experiments. *B*, the protein levels of Kap1 of cells in (*A*) were detected by Western blotting. β-Actin: loading control. *C*, Kap1 stable knockdown (shKap1-UTR) or negative control (shNC) cells expressing GFP-Pol η were complemented with Myc-Kap1 or not. Twenty-four hours later, the cells were exposed to ETO (2.5 μM) for 24 h. The proportions of GFP-Pol η–expressing cells with more than 30 foci were determined by counting at least 200 cells in each experiment. Data represent means ± SEM from three independent experiments. *D*, the protein levels of Kap1 and overexpressed Myc-Kap1 in (*C*) were detected by Western blotting. Tubulin: loading control. *E*, U2OS cells were transfected with FL (1–713) or truncated (301–713, 556–713 and 1–512) GFP-Pol η; 24 h later, the cells were exposed to ETO (2.5 μM) for 24 h. The proportions of GFP-Pol η–expressing cells with more than 30 foci were determined by counting at least 200 cells in each experiment. Data represent means ± SEM from three independent experiments. *F*, HEK293T cells transfected with FL or truncated (301–713, 556–713 and 1–512) GFP-Pol η were lysed and immunoprecipitated with anti-GFP agarose beads, followed by immunoblotting with anti-Kap1 and anti-GFP antibodies. ETO, etoposide.

dispersion after ETO treatment, with the proportions of 53BP1 foci–positive cells being significantly higher than those in WT cells (47.62% *versus* 32.63% at 2 h, 43.68% *versus* 21.41% at 10 h, and 30.84% *versus* 17.89% at 30 h) (Fig. 7*A*). However, Kap1 knockdown cells displayed an attenuated 53BP1 focus formation at 0 h after ETO exposure (Fig. S6*A*), echoing the previous report that Kap1 promotes 53BP1 loading at DSB sites (31). In addition, Rad18 or Kap1 knockdown cells displayed an impaired NHEJ repair efficiency (Fig. 7*B*) and increased sensitivity to ETO treatment (Fig. S6, *B* and *C*), indicating that, similar to Pol η, Rad18 and Kap1 facilitate NHEJ repair progression following ETO treatment.

It has been reported that phosphorylation of Rad18 on S409 and S434 by Dbf4/Drf1-dependent Cdc7 kinase (DDK) and

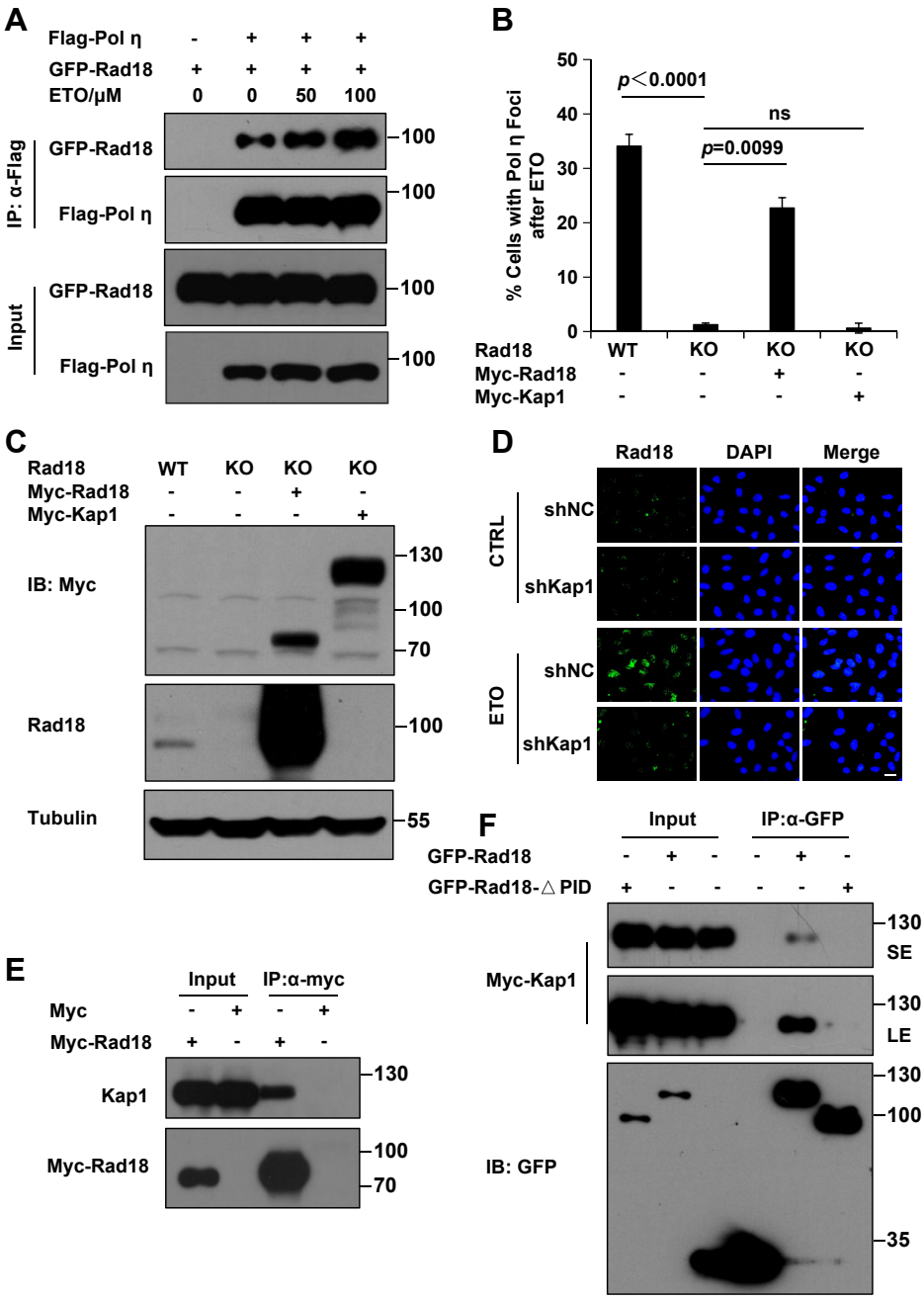

Figure 5. Kap1 regulates Pol η focus formation in a Rad18-dependent manner after ETO treatment. *A*, HEK293T cells expressing GFP-Rad18 and Flag-Pol η were treated with ETO (50 or 100 μM) for 2 h and further incubated for 2 h. The cells were lysed and immunoprecipitated using anti-Flag M2 agarose beads followed by Western blot using anti-GFP and anti-Flag antibodies. *B*, Rad18 wildtype (WT) or knockout (KO) U2OS cells transfected with GFP-Pol η and Myc-Rad18 or Myc-Kap1 were treated with ETO (2.5 μM) for 24 h. The proportion of GFP-Pol η–expressing cells with more than 30 foci was determined. Data represent means ± SEM from three independent experiments. *C*, the Rad18, Myc-Rad18, and Myc-Kap1 levels in (*B*) were detected by Western blot. Tubulin: loading control. *D*, representative images of cells stained with Rad18 after ETO treatment. U2OS cells were transfected with siKap1 or siNC oligos. Seventy hours later, the cells were treated with ETO (100 μM) for 3 h followed by immunostaining with anti-Rad18 antibody. Scale bar: 10 μm. *E*, HEK293T cells expressing Myc-Rad18 were lysed and immunoprecipitated using anti-Myc agarose beads. The immunoprecipitates were examined *via* Western blot using anti-Kap1 and anti-Myc antibodies. *F*, HEK293T cells were transfected with Myc-Kap1 and wildtype GFP-Rad18 or mutant GFP-Rad18-△PID (lacks Pol η–interacting domain). The cells were lysed and immunoprecipitated using anti-GFP agarose beads followed by Western blot using anti-Myc and anti-GFP antibodies. ETO, etoposide; SE, short exposure; LE, long exposure.

ATR/Chk1-dependent c-Jun N-terminal kinase promotes Rad18–Pol η association and facilitates Pol η recruitment to UV-induced damage sites for carrying out its TLS function (32). We wonder whether the phosphorylation of Rad18 was also required for optimal Pol η accumulation at ETO-induced DSBs. To test it, we transfected GFP-Pol η with WT or phosphorylation mutant (S409A/S434A) Rad18 into Rad18-deficient U2OS cells followed by ETO exposure. Notably, WT and S409A/S434A Rad18 manifested a comparable capacity in promoting Pol η focus formation (Fig. 7*C*) and in

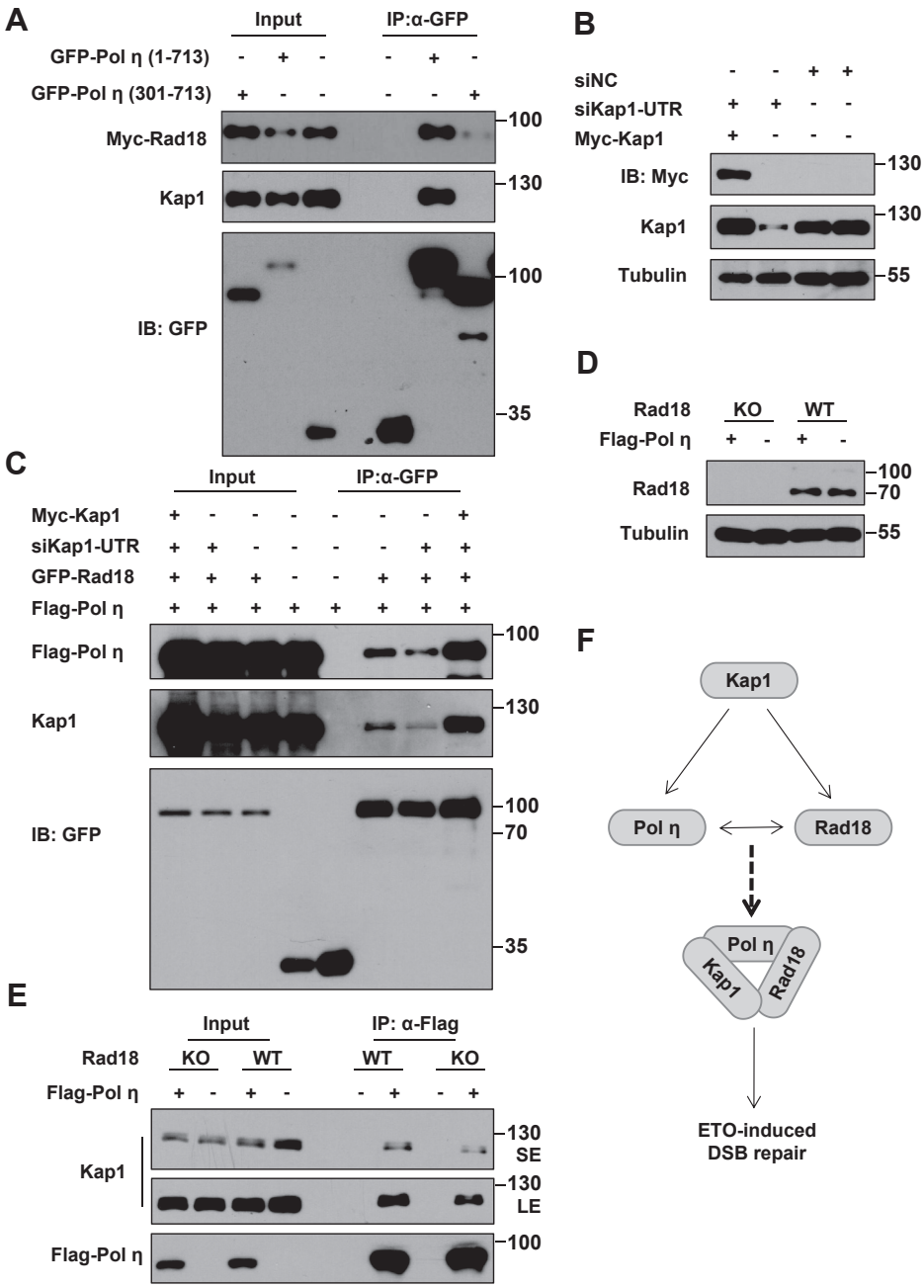

Figure 6. Kap1 forms a ternary complex with Rad18 and Pol η. *A*, HEK293T cells were transfected with Myc-Rad18 and WT GFP-Pol η or GFP-Pol η-301-713 (lacks Kap1-interacting domain). The cells were lysed and immunoprecipitated using anti-GFP agarose beads followed by Western blot using anti-Myc, anti-Kap1, and anti-GFP antibodies. *B*, the protein levels of Kap1 and Myc-Kap1 in (*C*) were detected by Western blotting. Tubulin: loading control. *C*, HEK293T cells were transfected with siKap1 or siNC oligos. Forty-eight hours later, the cells were transfected with Flag-Pol η, GFP-Rad18, and Myc-Kap1 or not. The cells were lysed and immunoprecipitated using anti-GFP agarose beads followed by Western blot using anti-Flag, anti-Kap1, and anti-GFP antibodies. *D*, the protein levels of Rad18 in (*E*) were detected by Western blotting. Tubulin: loading control. *E*, Rad18 WT or KO HEK293T cells were transfected with Flag-Pol η. The whole-cell lysates were immunoprecipitated with anti-Flag M2 agarose beads. The immunoprecipitates were immunoblotted with anti-Kap1 and anti-Flag antibodies. *F*, model of Pol η in ETO-induced DSB repair. Post ETO exposure, Kap1 promotes Rad18-dependent focus formation of Pol η by facilitating Rad18 recruitment and associating with Pol η, which forms a ternary complex to stabilize Rad18–Pol η association. DSB, double-strand break; ETO, etoposide; LE, long exposure; SE, short exposure.

binding with Pol η or Kap1 post ETO (Fig. S6, *D* and *E*), suggesting that ETO-induced Pol η focus formation and Kap1–Rad18–Pol η ternary complex formation are independent of Rad18 phosphorylation on S409/S434.

In addition to protein–protein interaction, protein post-translational modifications also fine-tune Pol η recruitment to stalled replication fork. In particular, ATR/PKC catalyzed phosphorylations on S587 and T617 have been reported to be required for Pol η recruitment after UV exposure (33). Given that Pol η accumulation at laser-induced damage sites was partially dependent on ATM (Fig. S1*B*), we asked whether Pol η phosphorylations on S587 and T617 also affected its focus

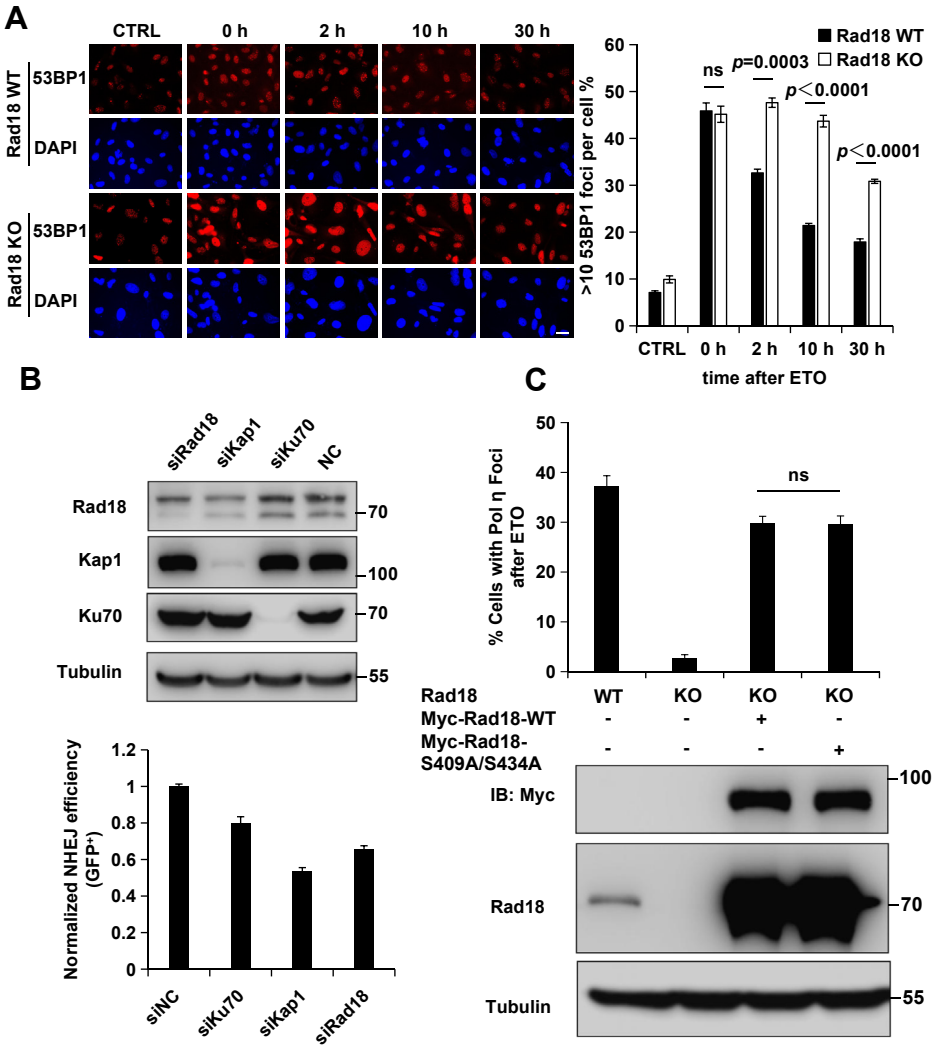

Figure 7. Rad18 and Kap1 promote NHEJ repair, while Rad18 phosphorylation on S409/S434 is not required for Pol η recruitment post ETO. *A*, representative images of cells stained with DAPI and 53BP1 after ETO treatment and quantification of the percentage of cells with more than 10 53BP1 foci. Rad18 WT and KO cells were treated with 50 μM ETO for 30 min and further cultured. At the indicated time points, cells were treated with 0.5% Triton-X100 for 10 min followed by immunofluorescence. For each cell line at each time point, at least 200 cells were counted. Data represent means ± SEM from three independent experiments. Scale bars: 10 μm. *B*, siRad18-, siKap1-, or siKu70-treated EJ5 cells were transfected with I-SceI endonuclease. NHEJ repair efficiency (GFP^+) was analyzed by FACS after 48 h. The *upper panels* show the immunoblots indicating the levels of Rad18, Kap1, and Ku70 in different conditions. Tubulin: loading control. *C*, Rad18 WT or KO U2OS cells transfected with GFP-Pol η and Myc-Rad18 (WT or S409A/S434A mutant) were treated with ETO (2.5 μM) for 24 h. The proportion of GFP-Pol η–expressing cells with more than 30 foci was determined. Data represent means ± SEM from three independent experiments. The *lower panels* show the immunoblots indicating the related Rad18 levels. Tubulin: loading control. ETO, etoposide; FACS, fluorescence activated cell sorting; NHEJ, nonhomologous end joining.

formation to ETO-induced DSBs. As is shown in Fig. S6*F*, Pol η-S587A and Pol η-T617A mutations significantly impaired Pol η focus formation post ETO compared WT control, providing direct evidence that Pol η phosphorylations on S587 and T617 are critical for its recruitment to DSBs following ETO treatment.

Discussion

Pol η plays an important role in genome maintenance through preventing replication fork stalling by allowing temporary bypass of DNA lesions. The well-known function of Pol η is to efficiently bypass cyclobutane pyrimidine dimer or Pt-GG adducts induced by UV or cisplatin. Defective Pol η is closely associated with the skin cancer–prone syndrome, xeroderma pigmentosum (34, 35). The findings that Pol η can also be utilized to act at intrinsically complicated tracks including D-loop extension to ensure chromosome stability (13, 36) modify the way of apprehending Pol η transactions on DNA damages, hinting the function of Pol η in DSB repair *via* distinct mechanisms. Although overexpression of Pol η has been reported to cause an increase in HR frequency, little effect on the HR frequency is observed when cells were depleted of Pol η (36, 37). What is more, it remains enigma whether Pol η function in NHEJ repair. Here, we found that Pol η colocalized with 53BP1 and γH2AX at microirradiated tracks and accumulated at ETO-induced DSB sites. By monitoring the time course of 53BP1 focus disappearance after ETO

treatment, we showed that Pol η depletion impaired ETO-induced DSB repair. Notably, Pol η knockdown resulted in a delayed 53BP1 focus dispersion in G1 phase, when NHEJ but not HR is operative. We also provided further evidence to support that Pol η could promote NHEJ repair in a non-catalytic fashion.

Based on MS analysis and Co-IP experiments, both DNA-PKcs and Kap1 were found to associate with Pol η. We noticed that Kap1 but not DNA-PKcs kinase activity is required for Pol η recruitment at ETO-induced DSBs. In addition to repressing transcription, Kap1 has been reported to be rapidly phosphorylated on S824 upon DNA damage to allow chromatin remodeling for efficient DNA repair in heterochromatin. Knockdown of Kap1 can decrease NHEJ repair efficiency as well as 53BP1 focus formation in cells (31). We found that Pol η could directly bind with Kap1 and colocalize with Kap1 S824p at microirradiated tracks. Notably, although the Kap1–Pol η interaction plays an important role in recruiting Pol η to ETO-induced DSB sites, ETO-induced Pol η focus formation was still regulated by Rad18, which seems to function downstream of Kap1 to modulate this process. In support of it, depletion of Kap1 significantly reduced the recruitment of Rad18 post ETO treatment. In addition, Kap1 supplementing could rescue the decreased Pol η focus formation in Kap1-depleted cells but not in Rad18-deficient cells after ETO treatment.

In this study, we also revealed that Rad18 accumulates at ETO-induced DSB sites along with Pol η. Moreover, ETO could promote Rad18–Pol η but not Kap1–Pol η association. Considering that the N-terminal and C-terminal of Pol η interact with Kap1 and Rad18, respectively, we speculated that Pol η, Kap1, and Rad18 might form a ternary complex. In support of this, we found that Kap1 associated with Rad18 in a Pol η–dependent manner and Rad18 depletion impaired the Kap1–Pol η association. Meanwhile, deletion of Kap1-binding domain in Pol η decreased its binding with Rad18. Therefore, Kap1 can promote Rad18-dependent Pol η focus formation at ETO-induced damage sites by facilitating Rad18 recruitment and enhancing Rad18–Pol η association. Notably, although the Rad18 phosphorylations on S409 and S434 by DDK/ATR/Chk1-dependent c-Jun N-terminal kinase can promote Rad18–Pol η association as well as UV-induced Pol η focus formation, it is not required for the Kap1–Rad18–Pol η ternary complex formation as well as efficient Pol η accumulation at ETO-induced DSBs. Moreover, depletion of Rad18 and Kap1 also caused a reduction in NHEJ efficiency as well as increased sensitivity to ETO, similar to those seen with Pol η knockdown.

In conclusion, we revealed that, beyond its TLS function, Pol η can also be involved in NHEJ and promote ETO-induced DSB repair under the modulation of Kap1 and Rad18. Briefly, upon ETO treatment, Kap1 gets phosphorylated to relax the chromatin and facilitate Rad18 recruitment, which then forms a ternary complex with Pol η and Kap1 to promote Pol η accumulation at DSBs and thereby NHEJ (Fig. 6*F*). Notably, ETO-induced Pol η focus formation is also regulated by its phosphorylations on S587 and T617, which was previously reported to be required for its recruitment to UV-induced stalled forks (33). Biophysical and structural data have shown that Kap1 forms antiparallel dimers *via* its tripartite motif (TRIM), which has key functional implications for the Kap1 network of interactions (38, 39). It is yet to be determined the specific domains of Kap1 that are responsible for its binding with Rad18 or Pol η. It will be of great value to illustrate the molecular mechanism in detail by which Kap1 enhances Rad18-Pol η accessibility after ETO exposure. Given that Pol η is upregulated in several types of cancer, such as glioblastoma multiforme, stomach adenocarcinoma, and cholangiocarcinoma, deeper understanding of Pol η functions in DSB repair holds a promise for improving the therapeutic efficacy.

Experimental procedures

Plasmids and reagents

Human full-length or truncations of Pol η cDNA were cloned in pGEX-4T-2, pEGFP-C3 (Clontech), or pCMV-2 × Flag-SBP (modified from pCMV-3 × Flag-myc) to generate GST, GFP, or Flag fusion proteins. Internal deletion mutants of pCMV-2 × Flag-SBP-Pol η were constructed as described (8). Human Kap1 cDNA was cloned into pGEX-4T-2 to generate GST-tagged Kap1. pET-28a-Pol η was a gift from Dr Wei Yang (NIDDK, National Institutes of Health). Myc-tagged RAD18 was a gift from Dr Jun Huang (Zhejiang University). Anti-Flag M2 (A2220) and anti-Myc (E6654) agarose affinity gel were purchased from Sigma (St Louis, MO). DNA-PKcs inhibitor Nu7026 (S2893) was from Selleckchem. Antibodies sources were as follows: mouse anti-Flag (F1804, 1:1000) from Sigma; anti-Pol η (ab17725, 1:1000), anti-γH2AX (ab11174, 1:1000), anti-Rad18 (ab57447, 1:1000), anti-DNA-PKcs (ab18356, 1:1000), and anti-Rad51 (ab133534, 1:200) from Abcam; anti-53BP1 (4937S, 1:1000) from Cell Signaling Technology; anti-Myc (MMS-150R-500, 1:1000) from Covance; anti-His (HT501–02, 1:1000) from Beijing TransGen Biotech Co, Ltd; anti-β-actin (M20010, 1:2000) from Abmart; anti-β-Tubulin (AbM59005–37-PU, 1:4000), anti-Ku80 (AbM51083-6-PU, 1:1000), and anti-Ku70 (AbM51079-4-PU, 1:1000) from Beijing Protein Innovation; anti-GFP (sc-8334, 1:500), anti-Kap1 (sc-515790, 1:1000), anti-PCNA (sc-56, 1:1000), and anti-PARP1 (sc-8007, 1:1000) from Santa Cruz Biotechnology. Alexa Fluor–conjugated secondary antibodies were from Invitrogen.

Cell culture and reagents

Human U2OS and HEK293T cells were obtained from the American Type Culture Collection. SV40-transformed MRC5 and XPV (XP30RO) fibroblast cells were kindly provided by Dr Alan Lehmann (40). GFP-Pol η–complemented XPV cell was constructed by lentiviral particles as described (8). Rad18 KO cells were established using transcription activator-like effector nuclease as described previously (41). These cell lines were grown in DMEM medium supplemented with 10% fetal bovine serum. All cells were grown at 37 °C in the presence of 5% CO_2 if not specified. All cells were tested for *Mycoplasma*

contamination using the Lonza *Mycoplasma* kit. For transient transfection experiments, cells were transfected with indicated constructs, using Vigofect (Vigorous Biotechnology) following the manufacturer's protocols.

For RNAi experiments, cells were transfected with siRNAs purchased from GenePharma using RNAiMAX (Invitrogen) according to the manufacturer's instruction and analyzed 72 h later. The gene-specific target sequences were as follows: Kap1-CDS (GAGAAUUAUUUCAUGCGUGAU), Kap1-UTR (CCUGGCUCUGUUCUCUGUCCU), Pol η-1 (CAGCCAAATGCCCATTCGCAA), Pol η-2 (CTGGTTGTGAGCATTCGTGTA), siRad18 (GAGCATGGATTATCTATTCAATT), si53BP1 (AGAACGAGGAGACGGTAATAGTGGG), siKu80 (GCGAGTAACCAGCTCATAA) and siKu70 (TTAGTGATGTCCAATTCA). The negative control (siNC) sequence (UUCUCCGAACGUGUCACGU) was also obtained from GenePharma. For shRNA knockdown, oligonucleotide encoding shRNA of Pol η were synthesized by Sangon. The oligonucleotides were annealed and cloned into pLKO.1 vector (Biovector) to generate shRNA-Pol η vectors. The shRNA sequences are as follows:

shPol η-CDS: CAGAAAGGCAGAAAGTTAATTCAAGAGATTAACTTTCTGCCTTTCTG, and shPol η-UTR: GAGATGAGGTTTCACCATGTTTTCAAGAGAAACATGGTGAAACCTCATCTC.

Laser microirradiation and imaging

The microirradiation was carried with a pulsed nitrogen laser (365 nm, 10-Hz pulse) as previously described (42–44). Briefly, U2OS cells were seeded on 35-mm glass bottom dishes (MatTek) overnight before transfection with GFP-Pol η. Cells were visualized with a Nikon Eclipse Ti-E inverted microscope equipped with a computer-controlled MicroPoint Laser Ablation System (Photonics Instruments). GFP-Pol η–expressing cells were selected for laser microirradiation. The frequency of cells that exhibit a visible accumulation of Pol η along the line of irradiation at 10 min after microirradiation was determined. Standard errors were derived from at least three independent experiments.

Immunofluorescence

Immunofluorescence was performed as described (8). Briefly, cells were cultured on glass coverslips and treated with etoposide as indicated. The cells were permeabilized with 0.5% Triton X-100 for 5 to 30 min before fixed in 4% paraformaldehyde. Then the cells were incubated with 5% fetal bovine serum for 45 min followed by incubation with indicated antibodies for 45 min. After staining with secondary antibodies (Alexa Fluor 568; Molecular Probes) for 1 h, coverslips were mounted in Vectashield mounting medium (Vector Laboratories) containing the nuclear stain 4, 6-diamidino-2-phenylindole. Images were acquired with a Leica DM5000 equipped with HCX PL S-APO 63 × 1.3 oil CS immersion objective (Leica) and processed with Adobe Photoshop 7.041. For quantitative analysis of ETO-induced Pol η focus formation, U2OS cells transfected with GFP-Pol η were treated with ETO (2.5 μM for 24 h) and fixed with 4% paraformaldehyde. Images were acquired using a Leica DM5000 (Leica) equipped with HCX PL S-APO 63 × 1.3 oil CS immersion objective (Leica). A minimum of 200 nuclei were analyzed for each treatment.

Mass spectrometry

HEK293T cells were transfected with 2 × Flag-Pol η and harvested after 48 h. After treatment with 0.1% Triton X-100 in buffer (10 mM Tris–HCl [pH 8.0], 150 mM NaCl, 1 mM $MgCl_2$, 10 mM $ZnCl_2$) for 20 min, the triton-insoluble fractions were lysed and incubated with anti-Flag M2 agarose to immunoprecipitate Flag-Pol η. The immunoprecipitated proteins were resolved by SDS-PAGE and stained with Coomassie Blue G250. Then, the gel was sliced into multiple pieces and digested in-gel in trypsin buffer (0.01 μg/μl trypsin with 50 mM NH_4HCO_3) at 37 °C for 16 h. After extracting from the gel, the peptide mixtures were dried and dissolved with buffer A (0.1% formic acid) for liquid chromatography coupled with tandem mass spectrometry (LC-MS/MS) analysis. The peptide mixtures were separated and analyzed by Q Exactive HF mass spectrometer (Thermo Fisher Scientific) equipped with an EASY-nLC 1200 system (Thermo Fisher Scientific). The samples were loaded onto a C18 trap column at a maximum pressure of 280 bar and eluted with a 28-min gradient with 3 to 32% of buffer B (80% acetonitrile with 0.1% formic acid, flow rate, ∼600 nl/min). Survey scans were performed with full scans (m/z 300–1500) in the Orbitrap analyzer at a resolution of 60,000 at m/z 200. The top 20 precursor ions were selected for fragmentation in the high-energy collision dissociation cell with a normalized collision energy of 27, and MS/MS was acquired in the Orbitrap analyzer at a resolution of 15,000 at m/z 200. The automatic gain control was set to 3×10^6 for full MS and 1×10^5 for MS/MS, with a maximum injection time of 80 ms and a dynamic exclusion of 60 s. The raw data were searched by Maxquant software (version 1.6.2.10) for protein identification and quantitation using the Andromeda search engine against the Uniprot human proteome (96,788 target sequences, release 01/19/2020). The following search parameters were used: (1) trypsin as protease with a maximum of two missed and/or nonspecific cleavages, (2) none of fixed modifications, and (3) oxidation of Met (+15.9949 Da) and acetylation (protein N-term) (+42.01056 Da) as variable modification. The mass tolerance was set to 20 ppm for precursor ions and 20 ppm for fragment ions. Search results were filtered at an false discovery rate of 1% at both the PSM and protein group levels. Chromatin-IP-MS raw data of Flag-Pol η have been deposited to Zenodo (https://doi.org/10.5281/zenodo.5830989).

Co-IP and Western blotting

HEK293T cells transfected with full-length or a series of truncated mutants of Flag-Pol η were harvested at 48 h post transfection and lysed with Hepes buffer (50 mM Hepes pH 7.5, 150 mM NaCl, 1 mM EDTA, 1 mM EGTA, 10% glycerol, 1% Triton X-100, 25 mM NaF, 10 μM $ZnCl_2$). The whole-cell

lysates were immunoprecipitated with anti-Flag M2 agarose beads. Samples were separated by SDS-PAGE and detected by immunoblotting with indicated antibodies.

GST pull-down assay

For interaction between His-Pol η and GST-Kap1, purified His-Pol η diluted in Hepes buffer were incubated with GST or GST-Kap1 for 2.5 h at 4 °C. After washing, the bound proteins were separated by SDS-PAGE and analyzed by Western blot with indicated antibodies.

Establishment of Kap1 and Pol η knockdown stable cell lines

Two pairs of oligonucleotide encoding shRNA of Kap1, one pair of oligonucleotide encoding shRNA of Pol η and one pair of a nontargeting control plasmid (shNC), were synthesized by Sangon. The oligonucleotides were annealed and cloned into pLKO.1 vector (Biovector) to generate shRNA-Kap1, shRNA-Pol η, or shNC vectors. Stable Kap1 knockdown or negative control clones were generated by infecting U2OS cells with polybrene-supplemented medium obtained from HEK293T packaging cells transfected with the shRNA-Kap1 or shNC. Individual clones were isolated by limiting dilution in media containing puromycin and screened for Kap1 expression levels with antibodies against Kap1. Stable Pol η knockdown or negative control cells were generated by infecting MRC5 cells with lentivirus obtained from HEK293T packaging cells transfected with the shPol η-CDS or shNC. The shRNA sequences of Kap1 are as follows:

shKap1-CDS: GACCACCAGTACCAGTTCTTATTCAAGAGATAAGAACTGGTACTGGTGGTC,

shKap1-UTR: CTCTGTTCTCTGTCCTGTCACTTCAAGAGAGTGACAGGACAGAGAACAGAG,

NHEJ reporter assay

The reporter cassette for detection of NHEJ established in HeLa cells was performed as described (23). To examine the effect of Pol η overexpression on NHEJ, the plasmid encoding the I-SceI endonuclease was cotransfected with Flag-Pol η or Flag vector and a DsRed-expressing plasmid (pDsRed2-N1) into NHEJ reporter cell lines by using Amaxa Nucleofector (Amaxa). For detecting Pol η knockdown on NHEJ, cells were treated with Pol η shRNA and transfected with I-SceI endonuclease encoding plasmid and pDsRed2-N1 after 48 h. NHEJ of I-SceI–induced DSBs results in the appearance of GFP^+ cells. To quantify NHEJ events, the cells were examined by flow cytometry on day 4 after transfection. To normalize for the efficiency of transfection, the ratio of GFP^+ to $DsRed^+$ cells was used as a measure of NHEJ efficiency. For NHEJ reporter established in EJ5 cells, cells treated with siRNA were transfected with I-SceI endonuclease encoding plasmid. Forty-eight hours later, the cells were harvested and examined by flow cytometry.

Cell survival assay

Cells were seeded into 6-cm dishes (∼200 cells/dish) in triplicate and allowed to adhere for 5 h. The cells were then treated with the indicated doses of ETO or ICRF-193 for 24 h at 37 °C. After treatment, cells were further incubated in complete medium for 7 to 10 days. Colonies were fixed and counted. The survival of genotoxin-exposed cells was determined by relating the cloning efficiency to that of an untreated control (8).

Statistical analysis

All statistical tests were determined with a two-sided Student's t test unless otherwise noted. p values were rounded to four decimal places, and differences were considered as statistically significant when $p < 0.05$.

Data availability

All data supporting the findings of this study are available from the corresponding authors on request.

Supporting information—This article contains supporting information.

Acknowledgments—The authors thank Dr Alan Lehmann for reagents.

Author contributions—C. G. and T. T. conceived the study and designed experiments. X. M. performed most of the experiments. C. W. performed NHEJ reporter analysis under the guidance of M. Z. B. Z. performed Rad51 IF. Z. C. constructed catalytically inactive Pol η mutant (D13A/E22A/D115A/E116A, Polη-CI) plasmid. X. M., C. G., and T. T. analyzed the data and wrote the manuscript. All authors read and approved the manuscript for publication.

Funding and additional information—This research was supported by the National Key Research and Development Program of China (2018YFA0108500), National Natural Science Foundation of China (31800684, 81921006, 82030033, 31970740), Postdoctoral Research Foundation of China (2021M703206), CAS Strategic Priority Research Program XDPB2004, Natural Science Foundation of Shanxi Province (201801D221281), the State Key Laboratory of Membrane Biology, and CAS Key Laboratory of Genomic and Precision Medicine.

Conflict of interest statement—The authors declare that they have no conflicts of interest with the contents of this article.

Abbreviations—The abbreviations used are: Co-IP, coimmunoprecipitation; DDK, Dbf4/Drf1-dependent Cdc7 kinase; DNA-PKcs, DNA-dependent protein kinase catalytic subunit; DSB, double-strand break; ETO, etoposide; GST, glutathione S-transferase; HR, homologous recombination; KO, knockout; Kap1, Krüppel-associated box–associated protein 1; MS, mass spectrometry; mUb-PCNA, mono-ubiquitinated proliferating cell nuclear antigen; NHEJ, nonhomologous end joining; PCNA, proliferating cell nuclear antigen; Pol η, polymerase eta; TLS, translesion DNA synthesis; UV, ultraviolet.

References

1. Albertella, M. R., Green, C. M., Lehmann, A. R., and O'Connor, M. J. (2005) A role for polymerase eta in the cellular tolerance to cisplatin-induced damage. *Cancer Res.* **65**, 9799–9806

2. Johnson, R. E., Prakash, S., and Prakash, L. (1999) Efficient bypass of a thymine-thymine dimer by yeast DNA polymerase, Poleta. *Science* **283**, 1001–1004
3. Kannouche, P. L., Wing, J., and Lehmann, A. R. (2004) Interaction of human DNA polymerase eta with monoubiquitinated PCNA: A possible mechanism for the polymerase switch in response to DNA damage. *Mol. Cell* **14**, 491–500
4. Ma, X., Tang, T. S., and Guo, C. (2020) Regulation of translesion DNA synthesis in mammalian cells. *Environ. Mol. Mutagen* **61**, 680–692
5. Arlett, C. F., Green, M. H., Rogers, P. B., Lehmann, A. R., and Plowman, P. N. (2008) Minimal ionizing radiation sensitivity in a large cohort of xeroderma pigmentosum fibroblasts. *Br. J. Radiol.* **81**, 51–58
6. Inui, H., Oh, K. S., Nadem, C., Ueda, T., Khan, S. G., Metin, A., Gozukara, E., Emmert, S., Slor, H., Busch, D. B., Baker, C. C., DiGiovanna, J. J., Tamura, D., Seitz, C. S., Gratchev, A., *et al.* (2008) Xeroderma pigmentosum-variant patients from America, Europe, and Asia. *J. Invest. Dermatol.* **128**, 2055–2068
7. Kannouche, P. L., and Lehmann, A. R. (2004) Ubiquitination of PCNA and the polymerase switch in human cells. *Cell Cycle* **3**, 1011–1013
8. Ma, X., L, H., Li, J., Wang, Y., Ding, Y. H., Shen, H., Yang, Y., Sun, C., Huang, M., Tu, Y., Liu, Y., Zhao, Y., Dong, M. Q., Xu, P., Tang, T. S., *et al.* (2017) Polη O-GlcNAcylation governs genome integrity during translesion DNA synthesis. *Nat. Commun.* **8**, 1941
9. Bergoglio, V., Boyer, A. S., Walsh, E., Naim, V., Legube, G., Lee, M. Y., Rey, L., Rosselli, F., Cazaux, C., Eckert, K. A., and Hoffmann, J. S. (2013) DNA synthesis by Pol η promotes fragile site stability by preventing under-replicated DNA in mitosis. *J. Cell Biol.* **201**, 395–408
10. Ogi, T., Limsirichaikul, S., Overmeer, R. M., Volker, M., Takenaka, K., Cloney, R., Nakazawa, Y., Niimi, A., Miki, Y., Jaspers, N. G., Mullenders, L. H., Yamashita, S., Fousteri, M. I., and Lehmann, A. R. (2010) Three DNA polymerases, recruited by different mechanisms, carry out NER repair synthesis in human cells. *Mol. Cell* **37**, 714–727
11. Sekimoto, T., Oda, T., Kurashima, K., Hanaoka, F., and Yamashita, T. (2015) Both high-fidelity replicative and low-fidelity Y-family polymerases are involved in DNA rereplication. *Mol. Cell Biol.* **35**, 699–715
12. Rattray, A. J., and Strathern, J. N. (2005) Homologous recombination is promoted by translesion polymerase poleta. *Mol. Cell* **20**, 658–659
13. McIlwraith, M. J., Vaisman, A., Liu, Y., Fanning, E., Woodgate, R., and West, S. C. (2005) Human DNA polymerase eta promotes DNA synthesis from strand invasion intermediates of homologous recombination. *Mol. Cell* **20**, 783–792
14. Nitiss, J. L. (2009) Targeting DNA topoisomerase II in cancer chemotherapy. *Nat. Rev. Cancer* **9**, 338–350
15. Pommier, Y., Leo, E., Zhang, H., and Marchand, C. (2010) DNA topoisomerases and their poisoning by anticancer and antibacterial drugs. *Chem. Biol.* **17**, 421–433
16. Kantidze, O. L., and Razin, S. V. (2007) Chemotherapy-related secondary leukemias: A role for DNA repair by error-prone non-homologous end joining in topoisomerase II - induced chromosomal rearrangements. *Gene* **391**, 76–79
17. Bohgaki, T., Bohgaki, M., and Hakem, R. (2010) DNA double-strand break signaling and human disorders. *Genome Integr.* **1**, 15
18. Mao, Z., Bozzella, M., Seluanov, A., and Gorbunova, V. (2008) DNA repair by nonhomologous end joining and homologous recombination during cell cycle in human cells. *Cell Cycle* **7**, 2902–2906
19. Chang, H. H. Y., Pannunzio, N. R., Adachi, N., and Lieber, M. R. (2017) Non-homologous DNA end joining and alternative pathways to double-strand break repair. *Nat. Rev. Mol. Cell Biol.* **18**, 495–506
20. Zhao, Y., Biertümpfel, C., Gregory, M. T., Hua, Y. J., Hanaoka, F., and Yang, W. (2012) Structural basis of human DNA polymerase η-mediated chemoresistance to cisplatin. *Proc. Natl. Acad. Sci. U. S. A.* **109**, 7269–7274
21. Chen, C. Y., Kawasumi, M., Lan, T. Y., Poon, C. L., Lin, Y. S., Wu, P. J., Chen, Y. C., Chen, B. H., Wu, C. H., Lo, J. F., Weng, R. R., Sun, Y. C., and Hung, K. F. (2020) Adaptation to endoplasmic reticulum stress enhances resistance of oral cancer cells to cisplatin by Up-regulating polymerase η and increasing DNA repair efficiency. *Int. J. Mol. Sci.* **22**, 355
22. Srivastava, A. K., Han, C., Zhao, R., Cui, T., Dai, Y., Mao, C., Zhao, W., Zhang, X., Yu, J., and Wang, Q. E. (2015) Enhanced expression of DNA polymerase eta contributes to cisplatin resistance of ovarian cancer stem cells. *Proc. Natl. Acad. Sci. U. S. A.* **112**, 4411–4416
23. Mao, Z., Seluanov, A., Jiang, Y., and Gorbunova, V. (2007) TRF2 is required for repair of nontelomeric DNA double-strand breaks by homologous recombination. *Proc. Natl. Acad. Sci. U. S. A.* **104**, 13068–13073
24. Durando, M., Tateishi, S., and Vaziri, C. (2013) A non-catalytic role of DNA polymerase η in recruiting Rad18 and promoting PCNA monoubiquitination at stalled replication forks. *Nucleic Acids Res.* **41**, 3079–3093
25. Chen, L., Zhu, X., Zou, Y., Xing, J., Gilson, E., Lu, Y., and Ye, J. (2015) The topoisomerase II catalytic inhibitor ICRF-193 preferentially targets telomeres that are capped by TRF2. *Am. J. Physiol. Cell Physiol.* **308**, C372–C377
26. Hendel, A., Krijger, P. H., Diamant, N., Goren, Z., Langerak, P., Kim, J., Reissner, T., Lee, K. Y., Geacintov, N. E., Carell, T., Myung, K., Tateishi, S., D'Andrea, A., Jacobs, H., and Livneh, Z. (2011) PCNA ubiquitination is important, but not essential for translesion DNA synthesis in mammalian cells. *PLoS Genet.* **7**, e1002262
27. Ulrich, H. D. (2009) Regulating post-translational modifications of the eukaryotic replication clamp PCNA. *DNA Repair (Amst)* **8**, 461–469
28. Goodarzi, A. A., Noon, A. T., Deckbar, D., Ziv, Y., Shiloh, Y., Löbrich, M., and Jeggo, P. A. (2008) ATM signaling facilitates repair of DNA double-strand breaks associated with heterochromatin. *Mol. Cell* **31**, 167–177
29. Despras, E., Sittewelle, M., Pouvelle, C., Delrieu, N., Cordonnier, A. M., and Kannouche, P. L. (2016) Rad18-dependent SUMOylation of human specialized DNA polymerase eta is required to prevent under-replicated DNA. *Nat. Commun.* **7**, 13326
30. Guérillon, C., Smedegaard, S., Hendriks, I. A., Mailand, N., and Nielsen, M. L. (2020) Multisite SUMOylation restrains DNA polymerase η interactions with DNA damage sites. *J. Biol. Chem.* **295**, 8350–8362
31. Kuo, C.-Y., Li, X., Stark, J. M., Shih, H.-M., and Ann, D. K. (2016) RNF4 regulates DNA double-strand break repair in a cell cycle-dependent manner. *Cell Cycle (Georgetown, Tex.)* **15**, 787–798
32. Hedglin, M., and Benkovic, S. J. (2015) Regulation of Rad6/Rad18 activity during DNA damage tolerance. *Annu. Rev. Biophys.* **44**, 207–228
33. Chen, Y. W., Cleaver, J. E., Hatahet, Z., Honkanen, R. E., Chang, J. Y., Yen, Y., and Chou, K. M. (2008) Human DNA polymerase eta activity and translocation is regulated by phosphorylation. *Proc. Natl. Acad. Sci. U. S. A.* **105**, 16578–16583
34. Busuttil, R. A., Lin, Q., Stambrook, P. J., Kucherlapati, R., and Vijg, J. (2008) Mutation frequencies and spectra in DNA polymerase eta-deficient mice. *Cancer Res.* **68**, 2081–2084
35. Yang, W. (2014) An overview of Y-Family DNA polymerases and a case study of human DNA polymerase η. *Biochemistry* **53**, 2793–2803
36. Sebesta, M., Burkovics, P., Juhasz, S., Zhang, S., Szabo, J. E., Lee, M. Y., Haracska, L., and Krejci, L. (2013) Role of PCNA and TLS polymerases in D-loop extension during homologous recombination in humans. *DNA Repair (Amst)* **12**, 691–698
37. Sharma, S., Hicks, J. K., Chute, C. L., Brennan, J. R., Ahn, J. Y., Glover, T. W., and Canman, C. E. (2012) REV1 and polymerase ζ facilitate homologous recombination repair. *Nucleic Acids Res.* **40**, 682–691
38. Tubbs, A. T., Dorsett, Y., Chan, E., Helmink, B., Lee, B.-S., Hung, P., George, R., Bredemeyer, A. L., Mittal, A., Pappu, R. V., Chowdhury, D., Mosammaparast, N., Krangel, M. S., and Sleckman, B. P. (2014) KAP-1 promotes resection of broken DNA ends not protected by γ-H2AX and 53BP1 in G_1-phase lymphocytes. *Mol. Cell Biol.* **34**, 2811–2821
39. Stoll, G. A., Oda, S. I., Chong, Z. S., Yu, M., McLaughlin, S. H., and Modis, Y. (2019) Structure of KAP1 tripartite motif identifies molecular interfaces required for retroelement silencing. *Proc. Natl. Acad. Sci. U. S. A.* **116**, 15042–15051
40. Kannouche, P., Broughton, B. C., Volker, M., Hanaoka, F., Mullenders, L. H., and Lehmann, A. R. (2001) Domain structure, localization, and

function of DNA polymerase eta, defective in xeroderma pigmentosum variant cells. *Genes Dev.* **15**, 158–172
41. Wang, Z., Huang, M., Ma, X., Li, H., Tang, T., and Guo, C. (2016) REV1 promotes PCNA monoubiquitylation through interacting with ubiquitylated RAD18. *J. Cell Sci.* **129**, 1223–1233
42. Uematsu, N., Weterings, E., Yano, K., Morotomi-Yano, K., Jakob, B., Taucher-Scholz, G., Mari, P. O., van Gent, D. C., Chen, B. P., and Chen, D. J. (2007) Autophosphorylation of DNA-PKCS regulates its dynamics at DNA double-strand breaks. *J. Cell Biol.* **177**, 219–229
43. Zhang, X., Lv, L., Chen, Q., Yuan, F., Zhang, T., Yang, Y., Zhang, H., Wang, Y., Jia, Y., Qian, L., Chen, B., Zhang, Y., Friedberg, E. C., Tang, T. S., and Guo, C. (2013) Mouse DNA polymerase kappa has a functional role in the repair of DNA strand breaks. *DNA Repair (Amst)* **12**, 377–388
44. Zhang, C., Zhou, B., Gu, F., Liu, H., Wu, H., Yao, F., Zheng, H., Fu, H., Chong, W., Cai, S., Huang, M., Ma, X., Guo, Z., Li, T., Deng, W., *et al.* (2022) Micropeptide PACMP inhibition elicits synthetic lethal effects by decreasing CtIP and poly(ADP-ribosyl)ation. *Mol. Cell*. https://doi.org/10.1016/j.molcel.2022.1001.1020